Photon-absorption cross sections between 3 and 30 MeV

N. K. Sherman, C. K. Ross, and K. H. Lokan*
Division of Physics, National Research Council, Ottawa, Ontario K1A OR6, Canada
(Received 5 October 1978; revised manuscript received 19 November 1979)

Photon absorption by Al, Ta, and Bi between 3 and 30 MeV was measured using as a photon spectrometer a photoneutron time-of-flight detector and a liquid deuterium target. The atomic cross sections of Ta and Bi at the lowest energies (and of Al at higher energies) agree with calculated values appearing in published tabulations but exceed them at 25 MeV by about 2% in Ta and 3% in Bi. Calculations by others using empirical Coulomb corrections and improved screening corrections to the cross section for pair production by the nucleus agree with experiment to within $(0.5 \pm 0.4)\%$. Best experimental values of the combined correction for Bi are given.

[NUCLEAR REACTIONS ^{27}Al, ^{181}Ta, ^{209}Bi; measured total photon absorption $\sigma_\gamma(E)$; observed GDR; deduced electron pair production $\sigma_K(E)$; $E = 3.0$ to 30.0 MeV; resolution 500 keV; deduced experimental values for Bi of the combined Coulomb and screening correction; ^{2}H(γ, n) LD_2/TOF spectrometer.]

INTRODUCTION

By time-of-flight detection of photoneutrons from liquid deuterium we have measured the transmission of 3 to 30 MeV γ rays through Al, Ta, and Bi. We find that the atomic absorption cross sections exceed calculated values listed in well-known tabulations by amounts which increase with the photon energy and the atomic number of the absorber. Experimental evidence has accumulated[1-3] showing that the photon absorption cross sections of heavy elements at intermediate energies have been underestimated in the tables.[4,5] The dominant contribution to the total cross section σ for energies above a few MeV is the cross section for production of electron pairs in the Coulomb field of the nucleus σ_K. The nuclear pair cross section as a function of photon energy ω has recently been calculated[6] using improved empirical Coulomb corrections[7] to the plane wave approximation and relativistic atomic form factors in the screening corrections. From our measured total cross sections which agree within experimental error with those measured at Mainz[3,6] (or in the case of Bi, with Pb measurements suitably scaled up) we have extracted values of $\sigma_K(\omega)$ which agree very closely with the improved calculated values.[6]

METHOD

The present experiment is the first one using the ^{2}H(γ, n) reaction which is able to furnish high quality total absorption data, although use of the deuteron to measure γ-ray energy goes back 40 years.[8] Our innovations are the use of a liquid deuterium (LD_2) target with a time-of-flight (TOF) detector, and rapid cycling of absorbers in and out of the γ beam for precise time periods.

The Ottawa spectrometer is described schematically in Fig. 1. The experiment consists in measuring as a function of ω the ratio of F, the photon flux transmitted by an absorber of known mass per unit area, to the flux F_0 incident on it. Then σ is obtained from the relation

$$F(\omega) = F_0(\omega) \exp[-n\sigma(\omega)], \quad (1)$$

where n is the number of atoms/cm^2 in the absorber. Whereas other γ spectrometers detect electrons amidst a high electron background, in the TOF method neutrons are detected after the beam pulse at a remote quiet location. The thin-walled plastic LD_2 holder we use, which has been described before,[8] adds little background and the spectrum is free of nuclear structure present in earlier TOF measurements using the ^{2}H(γ, n) method—the first[9] using a deuterated polyethylene target, the second in our laboratory[10] based on $(D_2O - H_2O)$ differences. Cycling the absorbers avoids normalization to a second spectrometer (as was done at Mainz[11] with Compton spectrometers). A continuous energy range is covered (an advantage over nuclear resonance absorption experiments[1] which can be performed only at certain discrete energies) without changing magnet settings as one does with pair[2] or Compton[3] spectrometers. At 6 MeV our energy resolution $\Delta\omega$ is 30 keV, comparable to that of Ge(Li) detectors which, moreover, cannot operate in a high intensity γ beam. At 20 MeV $\Delta\omega$ is 340 keV, still better than for NaI (Tl). In common with all ratio measurements of total cross section, experimental factors such as incident γ spectrum, neutron detector efficiency, photon absorption in the target chamber walls,

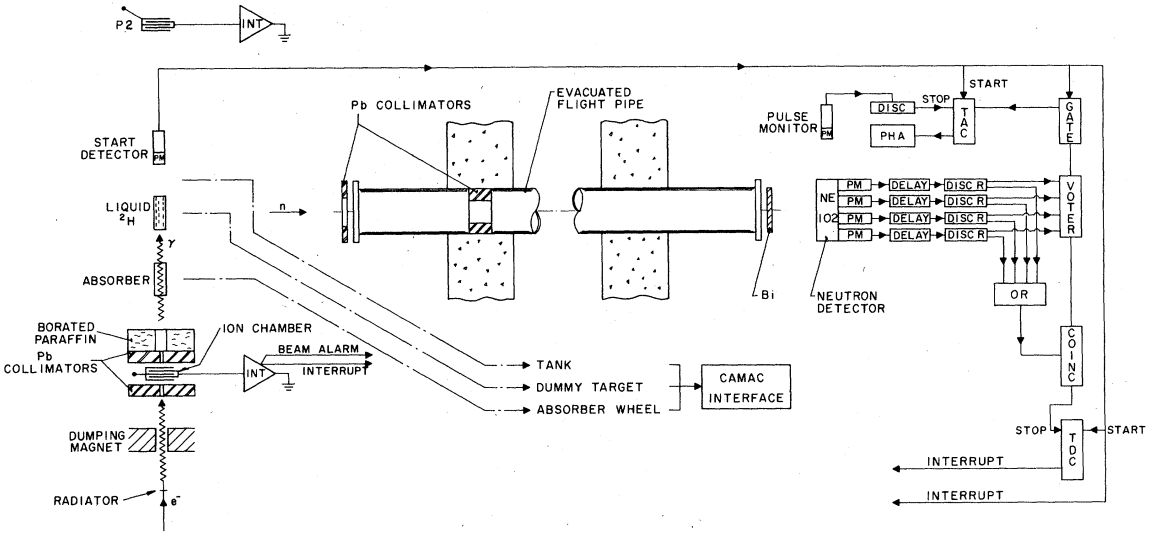

FIG. 1. Schematic diagram of the LD_2-TOF spectrometer. Three absorbers and a blank are mounted on a wheel ahead of the liquid deuterium (LD_2) target which is viewed by a TOF photoneutron detector. In the figure, e^- denotes the incident electron beam, γ the collimated photon beam, and n a photoneutron. The deuterium target is indicated by the label liquid ^{2}H, the standard ion chamber of Natl. Bur. Stand. (U.S.) design by $P2$, the bismuth γ-flash filter by Bi, and the plastic scintillator by NE 102. In the boxes representing electronic circuitry, the letters PM stand for photomultiplier tube, INT for current integrator, DISCR for discriminator, VOTER for majority-logic coincidence unit, COINC for coincidence unit, TDC for time digitizer, TAC for time-to-amplitude converter, and PHA for pulse height analyzer. The CAMAC interface permits computer-controlled cycling of the absorbers and alternation of the full target with an empty target. For background runs the vacuum tank (not shown) containing the LD_2 target is moved laterally and the dummy target descends into the photon beam. The pulse monitor is actually located on the flight pipe axis behind the neutron detector to record the average duration of the incident photon bursts. Photoneutron events (coincident pulses from 3 out of the 4 photomultipliers) are stored in time channels according to the interval between START and STOP pulses. The flight time reveals the neutron energy, so giving the photon energy.

and neutron absorption in the target or flight pipe windows cancel in the extraction of the experimental cross section $\sigma_{exp}(\omega)$.

A deuteron absorbing a photon of energy greater than the binding energy B (2.2246 MeV) disintegrates into a neutron and a proton with kinetic energies T_n and T_p uniquely related—so we need measure only T_n. If the photon is of low energy and a neutron moving perpendicular to the photon direction is detected, the simple relationship

$$\omega = 2T_n + B \tag{2}$$

gives the photon energy. In the present experiment, however, neutrons with energies of up to 20 MeV were detected requiring use of a relativistic version of (2). The flight time t of a neutron traversing a distance L, represented by τ in reduced units, is

$$t = (L/c)\tau\,, \tag{3}$$

where c is the speed of light. The kinetic energy of the neutron is

$$T_n = m_n[(1-\tau^{-2})^{-1/2} - 1]\,, \tag{4}$$

where m_n is the mass energy of the neutron. The photon energy is given by[12]

$$\omega = \frac{T_n[1+(m_n-B)/m_p] + B[1-(B/2m_p)]}{1-(T_n+B)/m_p + [T_n(T_n+2m_n)]^{1/2}\cos\theta/m_p}\,, \tag{5}$$

where m_p is the mass energy of the proton and θ is the laboratory angle between the photon beam direction and the direction of emission of the neutron.

EXPERIMENTAL PROCEDURE

The experimental arrangement is depicted in Fig. 1. Pulsed 42 MeV bremsstrahlung from the National Research Council of Canada (NRC) electron Linac irradiated the LD_2 target (47 mm diam., 15 cm long) axially. The γ beam was produced by $3A$, 720 Hz electron pulses of 8 ns duration striking a 0.5 mm Ta radiator. The LD_2 target was suspended in a large vacuum tank at a distance of 2.5 m from the radiator. Halfway between was a 4-armed wheel carrying three 54 mm diam. absorbers whose physical characteristics are listed in Table I. The fourth position was empty. Two Pb collimators each 5 cm thick placed ahead of the wheel restricted the photons to a pencil

TABLE I. Physical characteristics of the absorbers, including atomic number Z, purity by weight, and mass per unit area m. The measured densities ρ are compared with reference densities ρ_{ref}.

Element	Z	Purity (wt %)	m (g/cm^2)	ρ(g/cm^3)	ρ_{ref} (g/cm^3)
Al	13	99.995 [a]	47.86 ± 0.10	2.680 ± 0.008	2.6985 [d]
Ta	73	>99.9 [b]	30.25 ± 0.06	16.640 ± 0.050	16.6
Bi	83	>99 [c]	19.58 ± 0.04	9.745 ± 0.029	9.747

[a] Matrix of large single crystals: Mg(12 ppm), Si(10 ppm), Fe(10 ppm), Cu(30 ppm).
[b] Vacuum cast: principal impurity Nb(Z = 41).
[c] Vacuum cast: Cl(1 ppm), Fe(1 ppm), Ni(1 ppm), Cu(1 ppm), Ag(4 ppm), Sb(2 ppm), Pb(3 ppm), <1% As (Z = 33).
[d] Average of CRC Handbook value and Mainz (Ref. 3) value.

falling on the end of the LD_2 holder to prevent inscattering by those portions of the absorbers not directly shadowing the target. An empty holder suspended in the same vacuum tank as the LD_2 target was made to descend into the γ beam when the tank moved sideways to remove the LD_2 from the beam. This permitted background runs to be performed. The wheel, tank, and holder were moved by stepping motors controlled by a computer which also accumulated eight (γ,n) TOF spectra sequentially during each 6-min cycle; 1 min for each absorber position with full LD_2 target and 20 s for each position with empty holder. Data were rejected and the position remeasured if the beam intensity (measured by the first ion chamber) fell below about 85% of a set value during a cycle or if neutron events did not occur. Since the beam intensity changed with a time constant of the order of an hour, often several hours, variations were averaged over all target and absorber combinations. The number of beam pulses per cycle was constant to better than 1 in 43 200. The integrated current from the ion chamber between the collimators was independent of wheel position to within 0.03%.

Neutrons emitted at 90° were detected at the end of a 38.3 m evacuated flight path in a conventional recoil detector. A pulse from the detector signifying the arrival of a neutron stopped the rundown of a 1000-channel (4 ns/ch) time-to-digital converter (TDC) started by the photon pulse which produced the neutron. In this way the neutron flight time was measured. Figure 1 summarizes the detector electronics. No significant variations in neutron detector efficiency from cycle to cycle (monitored by the individual photomultiplier counting rates), or from run to run (monitored by the neutron detection threshold) were observed. Periodically, by inserting 7.62 cm of graphite in the TOF path, the TDC was calibrated against the 5 strongest and sharpest features in the $^{12}C(n,n')$ absorption spectrum. These are listed in Table II. The TDC calibration obtained from a linear least squares fit was then used to calculate the neutron energies for 8 features in the absorption spectrum (including the 5 used in the fit), given the time channel in which each feature was observed. Table II lists the photon energy which would be assigned to each of these time channels if the fitted calibration curve were used without further correction. The systematic error in all cases would be less than 60 keV between 6 and 18 MeV. In this energy region the photon energies have been further corrected by linear interpolation between the calibrating features, so the systematic error is estimated to be less than 30 keV. Above 18 MeV the possible systematic error is estimated to be 60 keV.

The observed full width at half maximum of the 2077 keV absorption line was 2 channels (8.8 ns) indicating that the time resolution of the TOF system was 0.23 ns/m. The photon energy resolution was therefore 38 keV at 6.3 MeV, worsening to 280 keV at 18 MeV and 484 keV at 25 MeV. In presenting the data in Tables III–V and Figs. 2 and 3, sufficient time channels have been added together to form energy bins of width approximately equal to 500 keV (2 time channels at 26 MeV).

The 2077 keV line was visible in all the neutron TOF spectra, due to neutron absorption by ^{12}C in the plastic scintillator of the TOF detector. The sharpness of the minimum provided a continuous check on the time stability of the TOF system. No drift was observed at any time. The threshold energy for neutron detection was 400 keV. This imposed a lower limit of 3 MeV on the photon energy which could be measured.

The elements studied were chosen because they are monoisotopic, span a fairly wide range of atomic number Z, can be obtained in very pure form, possess good dimensional stability, and have a well-defined, uniform density. The masses of the absorbers were measured to a precision of 0.1 mg (about 2 parts in 10^7) on a standards

TABLE II. Features in the $^{12}C(n,n')$ absorption cross section used to calibrate the time-of-flight system. The neutron kinetic energy T_n at which a feature appears and the neutron flight time t over a distance of 38.3 m are compared with T_f and t_f, the kinetic energy and time obtained from the fitted calibration curve. The photon energy ω assigned to photoneutrons emitted by deuterium at 90° and detected in a given channel is systematically in error by $\delta\omega$ when T_f differs from T_n. Photon energies in the other tables have been adjusted by linear interpolation to correct for this.

Channel No.	T_n (keV) [a]	t (ns)	t_f (ns)	T_f (keV)	ω (MeV)	$\delta\omega$ (MeV)
180	7758 ± 5 [b]	1000	1000	7770	17.765	+0.024
205	6293 ± 5 [b]	1109	1109	6295	14.815	+0.004
226	5366 ± 6	1200	1202	5356	12.936	−0.020
259.5	4260 ± 20	1346	1349	4247	10.718	−0.026
289	3600 ± 50	1464	1478	3533	9.290	−0.054
316	3010 ± 2 [bcd]	1600	1597	3025	8.275	+0.031
322	2950 ± 2 [b]	1616	1623	2922	8.069	−0.056
391	2077 ± 2 [b]	1925	1926	2076	6.278	−0.001

[a] S. F. Mughabghab and D. I. Garber, BNL 325, 3rd ed. (Brookhaven National Laboratory, U. S. Dept. of Commerce, Springfield, Virginia, 1973), p. 6-1.

[b] Used in best fit ($r^2 = 0.999\,967$, compared to 1.00 for a perfect fit), giving 4.388 25 ns/channel.

[c] R. B. Schwartz, R. A. Schrack, and H. T. Heaton, NBS Monograph 138 (National Bureau of Standards, U. S. Dept. of Commerce, Washington D. C., 1974), pp. 26, 27.

[d] Resonant minimum in the $^{12}C(n,n')$ cross section.

balance. For Al the accuracy was limited to 4 parts in 10^5 by uncertainty in the correction to the mass for air displacement. The absorber diameters were measured by micrometer to an accuracy of 0.1%. The mass per unit area was therefore uncertain to ±0.2%. As a check on the presence of appreciable voids which if distributed nonuniformly throughout the absorber volume (not all of which was traversed by photons) could lead to an error in the mass per unit area, the absorber lengths were measured by caliper to 0.1%. The densities obtained are compared in Table I with reference values. There is no reason to suspect that the Ta and Bi absorbers, which were vacuum cast, contain voids. Our measured density for Al is slightly smaller than the mean of the Mainz[3] and Chemical Rubber Company (CRC) handbook values (by about 0.6% which is only about twice our estimated measurement error). The Mainz sample, having been sawn up, is known to have been free of voids. Our sam-

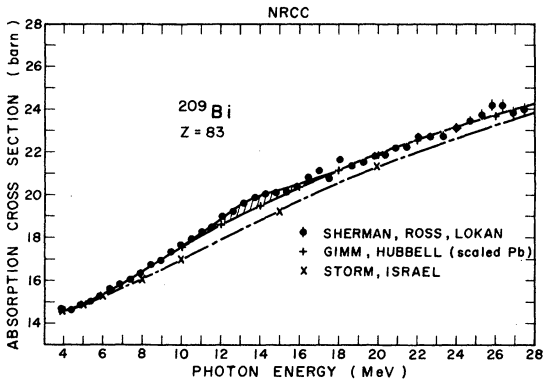

FIG. 2. The measured Bi photon absorption cross section is plotted (solid circles) against photon energy. The bars represent statistical error. The hatched area, the total (γ,n) cross section (Refs. 14 and 15), approximates the total photonuclear absorption. The crosses (+) represent the calculated (Ref. 6) atomic cross section of Pb scaled up to $Z = 83$. Previous calculations (Ref. 5) are denoted by (X).

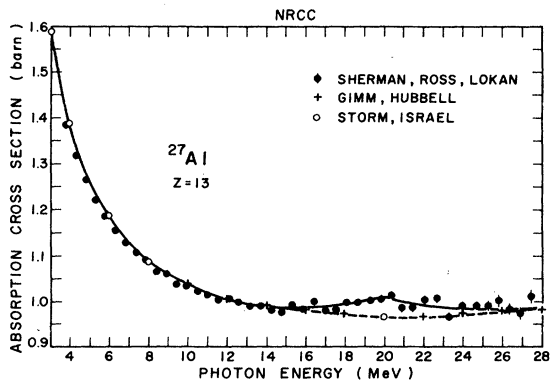

FIG. 3. The measured Al absorption cross section (solid circles) compared to the new (Ref. 6) (crosses) and old (Ref. 5) (open circles) theory. The excess above 15 MeV is photonuclear.

TABLE III. Measured values σ_{exp}(Ta) of the absorption cross section of tantalum and their statistical errors ϵ_σ are listed against photon energy ω along with the atomic cross sections σ_Z(Ta) and nuclear pair cross sections σ_K(Ta) obtained from them. Values of σ_Z interpolated from measurements made at Mainz [a] are shown for comparison. The amounts $\delta\sigma_Z$ and $\delta\sigma_K$ by which σ_Z(Ta) and σ_K(Ta) exceed the calculated [b] values σ_Z(calc) and σ_K(calc) are also given.

ω (MeV)	σ_{exp}(Ta) (b)	ϵ_σ (mb)	σ_Z(Ta) [c] (b)	$\delta\sigma_Z$ (mb)	σ_Z(Mainz) (b)	σ_K(Ta) (b)	σ_K(calc) (b)	$\delta\sigma_K$ (b)
3.869	12.126	±56	12.123	−57		4.47	4.45	+0.02
4.327	12.128	30.5	12.124	−66		5.04	5.05	−0.01
4.830	12.258	23.5	12.252	+8		5.82	5.67	+0.15
5.333	12.394	21	12.386	−4		6.26	6.23	+0.03
5.837	12.561	20.5	12.551	0		6.80	6.75	+0.05
6.348	12.789	21.5	12.777	+60		7.35	7.27	+0.08
6.870	12.990	21.5	12.974	+70		7.84	7.77	+0.07
7.404	13.171	22.5	13.149	+40		8.26	8.24	+0.02
7.936	13.391	24.5	13.365	+40		8.69	8.66	+0.03
8.382	13.601	26.5	13.564	+11		9.11	9.07	+0.04
8.936	13.854	28.5	13.807	+70		9.55	9.46	+0.09
9.476	14.079	30	14.019	+70		9.92	9.84	+0.08
9.992	14.318	32	14.240	+70	14.19	10.30	10.22	+0.08
10.514	14.507	34	14.405	+30	14.40	10.61	10.56	+0.05
11.039	14.775	36.5	14.635	+60	14.58	10.98	10.90	+0.08
11.557	15.056	40	14.828	+40	14.79	11.30	11.23	+0.07
12.088	15.380	41.5	15.052	+60	14.98	11.63	11.58	+0.05
12.629	15.562	46	15.194	0	15.17	11.88	11.88	0.00
13.174	15.730	47.5	15.386	−20		12.18	12.18	0.00
13.715	15.947	54	15.605	−20		12.48	12.46	+0.02
14.253	16.124	56.5	15.764	−50	15.81	12.70	12.76	−0.06
14.780	16.303	63	15.921	−80	16.02	12.93	13.02	−0.09
15.293	16.522	64.5	16.137	−50	16.23	13.21	13.27	−0.06
15.840	16.683	67.5	16.333	−40	16.40	13.48	13.50	−0.02
16.422	16.841	68.5	16.541	−10	16.57	13.76	13.77	−0.01
16.977	16.924	78	16.684	−30		13.97	14.00	−0.03
17.500	17.093	82.5	16.895	+20		14.25	14.22	+0.03
18.078	17.188	84	17.026	−30		14.44	14.46	−0.02
18.665	17.324	86.5	17.188	−20	17.25	14.72 [d]	14.66	+0.06
19.286	17.412	±90	17.294	−100	17.45	14.96 [d]	14.90	+0.06
19.856	17.920	112	17.816	+260	17.62	15.17 [d]	15.11	+0.06
20.370	17.850	112	17.758	+70	17.75	15.35 [d]	15.28	+0.07
20.907	17.868	115	17.785	−50	17.88	15.53 [d]	15.47	+0.06
21.468	17.903	117.5	17.829	−140				
22.055	18.316	124	18.252	+130				
22.670	18.362	127.5	18.306	+50				
23.314	18.380	131	18.333	−90				
23.989	18.791	136.5	18.751	+170				
24.697	18.514	137.5	18.480	−250				
25.312	18.709	176	18.679	−190				
25.825	18.658	177.5	18.632	−360				
26.355	19.156	187.5	19.132	+30				
26.903	19.300	195.5	19.277	+50				
27.470	19.408	206.5	19.387	+30				

[a] J. Ahrens *et al.* (Ref. 3). Numerical values are given in Ref. 6.

[b] Calculated atomic cross section values σ_Z(calc) were obtained by interpolation of tables compiled by J. H. Hubbell, H. A. Gimm, and I. Øverbø (private communication).

[c] Obtained by subtracting the total photoneutron cross section measured (Ref. 17) by R. Bergere *et al.* from σ_{exp}(Ta). See also Ref. 16.

[d] Using the interpolated Mainz (Ref. 6) value.

ple (consisting of 3 shorter cylinders) was cut from an ingot of such high purity that it consited of a uniform mosaic of large single crystals. No voids were encountered on the cuts, or during the machining of the cylinders. Further evidence for uniformity of the Al density is that the measured density of each cylinder differs from the mean value by no more than 0.12%.

DATA AND DISCUSSION

The TOF spectrum for each target-absorber combination was corrected for counting losses as described in Appendix A and normalized to the number of Linac pulses which produced it. Then the empty target spectrum with or without absorber was subtracted from the corresponding full target spectrum.

For a given absorber having n atoms/cm^2 experimental values σ_{exp} of the cross section are obtained from the subtracted TOF spectra: The time bin corresponding to photon energy ω [see (4) and (5)] gives, using (1),

$$\sigma_{\text{exp}}(\omega) = \{\ln[N_0(\omega)/N(\omega)]\}/n\,, \tag{6}$$

where N and N_0 are the corrected, normalized numbers of events in this bin (two or more time channels added together, as mentioned earlier) with and without the absorber in the beam.

The measured cross section values and their statistical errors ϵ_σ are listed in Tables III, IV, and V. Where necessary the cross section value given by (6) was corrected for in-scattering and air displacement. The combined correction amounted to an increase of 0.2% for Al, and was negligible for Ta and Bi. In-scattering is discussed in more detail in Appendix B. Displacement of air by the absorber prevents complete cancellation in the ratio in Eq. (6) of the effect of photon absorption in the air path between radiator and LD_2 target. The apparent reduction in cross section is easily calculated to be 0.08% at 3 MeV for the Al absorber, decreasing to 0.04% at higher energy.

In the case of a heavy element the total photoneutron cross section σ_n at a given energy is expected to be a good approximation to σ_N, the total nuclear absorption cross section at the same energy. Since

$$\sigma_{\text{exp}} = \sigma_Z + \sigma_N\,, \tag{7}$$

where σ_Z is the sum of all the atomic cross sections, we can write in the case of Ta and Bi, at each energy,

$$\sigma_Z = \sigma_{\text{exp}} - \sigma_n\,. \tag{8}$$

The measured values of σ_Z obtained from (8) are compared to the new calculations[6] in the tables. The Ta results are compared to measurements[3,6] made at Mainz. The Bi results are compared to Pb results from Mainz scaled up by the ratio of σ_Z (Bi) to σ_Z (Pb) calculated by Gimm and Hubbell.[6] Figure 2 shows that σ_Z for Bi agrees around 3 MeV with the tabulation by Storm and Israel[5] (which they produced by interpolating in Z and ω from Hubbell's calculations[4]). Agreement at low energy between measurements and these calculated values has been observed previously.[13] However, as ω increases our measured σ_Z rises above the old calculated curves. The "scaled up Pb" points in the figure were obtained by multiplying the Rayleigh, photoelectric, Compton, triplet, and nuclear pair cross sections calculated[6] by Gimm and Hubbell for Pb by the appropriate powers of (83/82) and plotting their sum. The calculated values listed in the tables have been interpolated from an unpublished compilation by Hubbell, Gimm, and Øverbø which includes the case of $Z = 83$. The hatched area in Fig. 2 represents σ_n which has been measured by two groups.[14,15] It should be noted that the data from Young's thesis[15] has been used in the tables. The Livermore (γ,n) cross section[14] is systematically smaller by several percent. This difference would be visible in Fig. 2 only in the vicinity of the giant dipole resonance (where it would be about the width of the solid lines). In the case of Bi also, two measurements of σ_n have been reported.[16,17] Again, we have used the larger[17] values to obtain σ_Z.

The Al data is shown in Fig. 3, and the absorption cross section below the photonuclear giant resonance is compared to calculations in Table V. The table shows that σ_{exp} for Al, corrected upwards by 0.2% for in-scattering and air displacement, lies on the average about 0.35% or approximately one standard deviation (imposed by uncertainty in the absorber area) below the calculated values in the energy interval 7 to 13 MeV, and about 1% below them between 4 and 7 MeV. The discrepancy appears to decrease systematically from 1.9% below 4 MeV to about zero at 13 MeV. The theoretical uncertainty is believed to be less than 0.2% for low-Z elements. Nevertheless the discrepancy appears to be real below 9 MeV. In support of this we note that Moreh and Wand[1] obtained (1147 ± 3) mb for the total Al cross section at 6.418 MeV, compared to (1152 ± 2) mb obtained by interpolation of our results—a discrepancy of only (5 ± 5) mb, or 0.4%, between the two experiments. Above 9 MeV, however, the agreement is very good between the calculated cross sections and our measurement modified by small in-scattering corrections. This gives us confidence in the soundness of the Ta and Bi measurements where the corrections are smaller still. We are

TABLE IV. Measured values σ_{exp}(Bi) of the absorption cross section of bismuth and their statistical errors ϵ_σ are listed against photon energy ω along with the atomic cross sections σ_Z(Bi) and nuclear pair cross sections σ_K(Bi) obtained from them. The amounts $\delta\sigma_Z$ and $\delta\sigma_K$ by which σ_Z(Bi) and σ_K(Bi) exceed the calculated [a] values σ_Z(calc) and σ_K(calc) are also given.

ω (MeV)	σ_{exp}(Bi) (b)	ϵ_σ (mb)	σ_Z(Bi) [b] (b)	$\delta\sigma_Z$ (mb)	σ_K(Bi) (b)	σ_K(calc) (b)	$\delta\sigma_K$ (b)
3.869	14.846	±76.5	14.841	+103	5.854	5.80	+0.05
4.327	14.781	44.5	14.775	−25	6.500	6.52	−0.02
4.830	14.927	33.5	14.919	−6	7.282	7.30	−0.02
5.333	15.091	30.5	15.081	−54	7.961	8.00	−0.04
5.837	15.324	29.5	15.311	−39	8.649	8.70	−0.05
6.348	15.624	31	15.606	+36	9.311	9.28	+0.03
6.870	15.878	32	15.856	+44	9.919	9.85	+0.07
7.404	16.100	33.5	16.072	−15	10.422	10.42	0
7.936	16.412	37	16.377	+27	10.987	10.96	+0.03
8.382	16.810	39	16.763	+158	11.613	11.48	+0.13
8.936	17.013	42.5	16.953	+63	12.028	11.96	+0.07
9.476	17.402	45	17.324	+174	12.574	12.42	+0.15
9.992	17.673	47.5	17.571	+166	13.004	12.92	+0.08
10.514	17.945	50	17.807	+132	13.407	13.30	+0.11
11.039	18.293	54	18.105	+145	13.880	13.75	+0.13
11.557	18.583	58.5	18.316	+91	14.229	14.12	+0.11
12.088	19.137	60.5	18.770	+283	14.803	14.55	+0.25
12.629	19.244	66	18.744	−6	14.919	14.92	0
13.174	19.669	68.5	19.049	+49	15.334	15.33	0
13.715	19.861	76.5	19.219	−46	15.619	15.66	−0.04
14.253	20.095	80.5	19.575	+40	16.088	16.02	+0.07
14.780	20.165	89	19.695	−90	16.280	16.32	−0.04
15.293	20.299	90.5	19.922	−90	16.585	16.64	−0.06
15.840	20.428	93	20.143	−92	16.893	16.95	−0.06
16.422	20.738	94.5	20.523	+58	17.343	17.24	+0.10
16.977	21.082	108.5	20.910	+223	17.805	17.56	+0.24
17.500	20.972	112	20.830	−70	17.785	17.85	−0.10
18.078	21.532	116	21.413	+303	18.438	18.14	+0.30
18.665	21.395	118	21.295	−30	18.385	18.41	+0.03
19.286	21.513	122	21.428	−117	18.578	18.69	−0.11
19.856	21.905	146.5	21.833	+78	19.033	18.96	+0.07
20.370	22.147	148.5	22.086	+156	19.341	19.17	+0.17
20.907	22.286	154	22.232	+122	19.532	19.41	+0.12
21.468	22.247	157	22.198	−87	19.553	19.62	+0.07
22.055	22.589	161	22.544	+57	19.944	19.87	+0.07
22.670	22.862	167.5	22.822	+157	20.277	20.08	+0.20
23.314	22.906	170.5	22.871	+4	20.384	20.34	+0.04
23.989	23.098	173	23.067	+2	20.630	20.60	+0.03
24.697	23.348	182	23.318	+48	20.923	20.85	+0.07
25.312	23.504	229.5	23.476	+26	21.126	21.08	+0.05
25.825	24.074	239.5	24.049	+462	21.724	21.27	+0.45
26.355	24.281	242	24.258	+521	21.958	21.45	+0.50
26.903	23.803	247	23.782	−108	21.502	21.62	−0.12
27.470	24.142	251	24.122	+62	21.852	21.80	+0.05

[a] Calculated atomic cross section values σ_Z(calc) were obtained by interpolation of tables compiled by J. H. Hubbell, H. A. Gimm, and I. Øverbø (private communication).

[b] Obtained by subtracting the total photoneutron cross section measured (Ref. 15) by L. M. Young from σ_{exp}(Bi). See also Ref. 14.

on firm ground for asserting that discrepancies between measurement and the earlier tabulations for large Z and ω arise from assumptions made in the calculations.

Tables III and IV compare σ_Z for Ta and Bi with σ_Z (calc) obtained by interpolation of values found in Ref. 6. The discrepancy $\delta\sigma_Z$ is listed, where

$$\delta\sigma_Z = \sigma_Z - \sigma_Z(\text{calc}). \tag{9}$$

TABLE V. Values σ_A and σ_B of the Al absorption cross section obtained from different data sets A and B for photon energies ω below the photonuclear giant resonance. Data set A was accumulated in about one-quarter the time required for data set B, at an average counting rate about 4% higher. The difference $\delta_{AB}\sigma$ between the two measurements is listed, as are σ_{AB}(Al) obtained by statistically weighting both data sets, σ_{calc} interpolated from a table [a] of calculated values, and $\delta\sigma$ the difference between σ_{calc} and the experimental values σ_{exp}(Al) obtained from σ_{AB}(Al) by correcting for in-scattering and air displacement.

ω (MeV)	σ_A (b)	σ_B (b)	$\delta_{AB}\sigma$ (mb)	σ_{AB}(Al) (b)	σ_{exp}(Al) (b)	σ_{calc} (Al) (b)	$\delta\sigma$ (mb)
3.873	1.398 ± 0.0075	1.385 ± 0.007	+13	1.388 ± 0.007	1.391	1.418	27
4.327	1.338 ± 0.0075	1.323 ± 0.0035	+15	1.326 ± 0.004	1.329	1.354	25
4.830	1.272 ± 0.005	1.272 ± 0.0025	0	1.272 ± 0.003	1.274	1.293	19
5.333	1.233 ± 0.004	1.226 ± 0.002	+7	1.228 ± 0.002	1.230	1.244	14
5.837	1.187 ± 0.0035	1.186 ± 0.002	+1	1.186 ± 0.002	1.188	1.202	14
6.348	1.150 ± 0.0035	1.154 ± 0.002	−4	1.153 ± 0.002	1.155	1.167	12
6.870	1.126 ± 0.0035	1.130 ± 0.002	−4	1.129 ± 0.002	1.131	1.139	8
7.404	1.106 ± 0.004	1.107 ± 0.002	−1	1.107 ± 0.002	1.109	1.115	6
7.936	1.085 ± 0.004	1.089 ± 0.002	−4	1.088 ± 0.002	1.090	1.097	7
8.382	1.068 ± 0.0045	1.067 ± 0.002	+1	1.067 ± 0.002	1.069	1.079	10
8.936	1.059 ± 0.0045	1.058 ± 0.0025	+1	1.058 ± 0.002	1.060	1.062	2
9.476	1.045 ± 0.005	1.038 ± 0.0025	+7	1.040 ± 0.002	1.042	1.051	9
9.992	1.036 ± 0.005	1.035 ± 0.003	+1	1.035 ± 0.003	1.037	1.040	3
10.514	1.022 ± 0.005	1.023 ± 0.0025	−1	1.023 ± 0.003	1.025	1.029	4
11.039	1.019 ± 0.0055	1.015 ± 0.003	+4	1.016 ± 0.003	1.018	1.018	0
11.557	1.008 ± 0.006	1.004 ± 0.003	+4	1.005 ± 0.003	1.007	1.009	2
12.088	0.985 ± 0.006	1.003 ± 0.003	−18	0.999 ± 0.003	1.001	1.001	0
12.629	0.995 ± 0.0065	0.995 ± 0.0035	0	0.995 ± 0.004	0.997	0.995	−2

[a] J. Hubbell, H. Gimm, and I. Øverbø (private communication).

At Mainz σ_Z has been measured for Ta over three intervals of photon energy lying within the energy range studied in this experiment. Interpolation of the data of Ahrens *et al.* (given in Ref. 6) provides values of σ_Z which agree very well with the present data, as Table III shows.

Similarly if the values of the total absorption cross section for Pb measured at Mainz are scaled up according to the ratio of calculated[6] atomic cross sections (a factor of 1.020 applies over most of the photon energy range) they agree closely with our measured values where the two data sets overlap.

A set of experimental values of σ_K, the cross section for electron pair production on the nucleus, was obtained by subtracting from σ_Z the sum of the calculated atomic cross sections (photoelectric, Compton, Rayleigh, and triplet):

$$\sigma_K = \sigma_Z - (\sigma_{pe} + \sigma_C + \sigma_R + \sigma_t) . \tag{10}$$

The cross sections in the parentheses in (10) have been recalculated by Hubbell, Gimm, and Øverbø.[6] The new values do not differ materially from older ones and are presumed to be accurate to better than 0.2%. The measured nuclear pair cross section σ_K is compared in Tables III and IV with σ_K(calc) obtained by Hubbell *et al.* using relativistic atomic form factors in the screening correction as well as the Øverbø estimate of the Coulomb correction. The discrepancy $\delta\sigma_K$ is tabulated, where

$$\delta\sigma_K = \sigma_K - \sigma_K(\text{calc}) . \tag{11}$$

Table VI compares for Bi the average $\bar{\sigma}_K$ of the Ottawa and "Mainz" (rescaled) values of σ_K with σ_K(calc). The unscreened, point nucleus, Born approximation prediction of the nuclear pair cross section at intermediate energies is[18]

$$\sigma_K = (\sigma_0\{28[\lambda - f(Z)]/9 - 218/27 + \Delta M\} + \Delta C' + \Delta S) f_{\text{rad}} , \tag{12}$$

where the curly-bracket term is the Davies-Bethe-Maximon cross section σ_{DBM}. The fine structure constant α and the classical radius of the electron r_0 are contained in

$$\sigma_0 = Z^2 \alpha r_0^2 , \tag{13}$$

and the photon energy, expressed in terms of the electron mass energy m as

$$k = \omega/m , \tag{14}$$

enters logarithmically via

$$\lambda = \ln 2k . \tag{15}$$

The correction term ΔM added to the Bethe-Heitler

TABLE VI. The measured values $\bar{\sigma}_K$ of the electron pair cross section on the Bi nucleus (above 9.5 MeV, the mean of Ottawa values for Bi, and Mainz values for Pb rescaled and interpolated) are compared with σ_K(calc) obtained (Ref. 6) by Hubbell, Gimm, and Øverbø at each photon energy ω. Also listed are the Davies-Bethe-Maximon cross section σ_{DBM}, $\bar{\sigma}_K$ divided by the radiative correction f_{rad}, the experimental values of the combined correction $(\Delta C' + \Delta S)$ for the energy dependent part of the Coulomb correction plus the screening correction, and the combined correction expressed as a fraction of the Bethe-Heitler cross section σ_{BH}.

ω (MeV)	$\bar{\sigma}_K$ (b)	σ_K(calc) (b)	σ_{DBM} (b)	$\bar{\sigma}_K/f_{\mathrm{rad}}$ (b)	$(\Delta C' + \Delta S)$ (b)	$\frac{(\Delta C' + \Delta S)}{\sigma_{\mathrm{BH}}}$
3.869	5.854	5.80	0.9556	5.742	4.786	3.151
4.327	6.500	6.52	1.7685	6.338	4.570	1.571
4.830	7.282	7.30	2.5791	7.171	4.592	1.074
5.333	7.961	8.00	3.3111	7.855	4.544	0.8255
5.837	8.649	8.70	3.9740	8.536	4.562	0.6885
6.348	9.311	9.28	4.5825	9.191	4.608	0.6010
6.870	9.919	9.85	5.1459	9.793	4.647	0.4745
7.404	10.422	10.42	5.6690	10.291	4.622	0.4825
7.936	10.987	10.96	6.3021	10.850	4.548	0.4356
8.382	11.613	11.48	6.9274	11.470	4.543	0.4119
8.936	12.028	11.96	7.8452	11.881	4.036	0.3387
9.476	12.536	12.42	8.5986	12.384	3.785	0.2994
9.992	12.956	12.92	9.2748	12.800	3.525	0.2650
10.514	13.410	13.30	9.9206	13.248	3.327	0.2388
11.039	13.871	13.75	10.5358	13.704	3.168	0.2179
11.557	14.238	14.12	11.1125	14.067	2.954	0.1955
12.088	14.725	14.55	11.6755	14.549	2.874	0.1834
12.629	14.935	14.92	12.2226	14.758	2.535	0.1564
13.174	15.312	15.33	12.7493	15.132	2.383	0.1424
13.715	15.769	15.66	13.2500	15.496	2.246	0.1303
14.253	16.126	16.02	13.7277	15.940	2.212	0.1249
14.780	16.343	16.32	14.1778	16.155	1.977	0.1089
15.293	16.636	16.64	14.6003	16.445	1.845	0.0992
15.840	16.939	16.95	15.0350	16.745	1.710	0.0899
16.422	17.324	17.24	15.4808	17.126	1.645	0.0845
16.977	17.704	17.56	15.8910	17.503	1.612	0.0811
17.500	17.829	17.85	16.2654	17.627	1.362	0.0672
18.078	18.302	18.14	16.6659	18.095	1.429	0.0692
18.665	18.403	18.41	17.0597	18.196	1.136	0.0539
19.286	18.642	18.69	17.4627	18.432	0.969	0.0451
19.856	18.993	18.96	17.8212	18.780	0.959	0.0439
20.370	19.258	19.17	18.1358	19.042	0.906	0.0409
20.907	19.469	19.41	18.4559	19.252	0.796	0.0354
21.468	19.605	19.62	18.7816	19.386	0.604	0.0265
22.055	19.925	19.87	19.1134	19.703	0.590	0.0255
22.670	20.209	20.08	19.4515	19.984	0.532	0.0227
23.314	20.400	20.34	19.7959	20.174	0.378	0.0159
23.989	20.656	20.60	20.1467	20.427	0.280	0.0116
24.697	20.934	20.85	20.5042	20.703	0.199	0.0081
25.312	21.144	21.08	20.8066	10.911	0.104	0.0042
25.825	21.531	21.27	21.0532	21.294	0.241	0.0096
26.355	21.736	21.45	21.3029	21.497	0.194	0.0077
26.903	21.594	21.62	21.5559	21.356	−0.200	−0.0078
27.470	21.856	21.80	21.8122	21.616	−0.196	−0.0076

terms of σ_{DBM} is due to Maximon[19]:

$$\Delta M = KA - K^2B - K^3C\,, \tag{16}$$

where

$$K = (2/k)^2\,, \tag{17}$$

and the coefficients of (16) are

$$A = (\tfrac{2}{3})\lambda^3 - \lambda^2 - (\pi^2/3 - 6)\lambda + \pi^2/6 - \tfrac{7}{2} + 2\zeta(3)\,, \tag{18a}$$

$$B = (3/16)\lambda + \tfrac{1}{8}, \tag{18b}$$

$$C = (29/2304)\lambda - (77/13\,824), \tag{18c}$$

and $\zeta(3)$ is 1.2 020 569. In (12), ΔS is the screening correction. The Coulomb correction ΔC contributes two terms to (12) and is given by

$$\Delta C = -(28/9)\sigma_0 f(Z) + \Delta C', \tag{19}$$

where $\Delta C'$ vanishes in the extreme relativistic limit, and

$$f(Z) = a^2 \sum_{n=1}^{\infty} [1/n(n^2 + a^2)] \tag{20}$$

with

$$a = Z\alpha. \tag{21}$$

The radiative correction in (12) is given by[6]

$$f_{\text{rad}} = 1 + 0.0093(\ln 2k - 1.58)/(\ln 2k - 2.08). \tag{22}$$

Table VI lists the experimental average cross section $\bar{\sigma}_K$ for Bi alongside the values calculated by Hubbell, Gimm, and Øverbø. The agreement is excellent. However, the ΔC used in the calculations is empirical, and is uncertain by about 10% according to Maximon and Gimm.[20] It is difficult to calculate it exactly. We can usefully, therefore, obtain from $\bar{\sigma}_K$ a list of experimental values of the sum of the screening correction plus the energy-dependent Coulomb correction. This sum of corrections is obtained from the experimental data by means of

$$(\Delta C' + \Delta S) = (\sigma_K / f_{\text{rad}} - \sigma_{\text{DBM}}). \tag{23}$$

Its values are listed in Table VI. It has also been expressed as a fraction of the Bethe-Heitler cross section σ_{BH}, where

$$\sigma_{\text{BH}} = \sigma_0(28\lambda/9 - 218/27), \tag{24}$$

in the last column of the table.

It should be noted that we have used one of Maximon's expansions,

$$\sigma_K^M = (2\pi/3)\sigma_0[(k-2)/k]^3[1 + \epsilon/2 + 23\epsilon^2/40 + 37\epsilon^3/210 + \cdots], \tag{25}$$

where

$$\epsilon = (k-2)/(k+2), \tag{26}$$

to calculate σ_{DBM} at small values of k using

$$\sigma_{\text{DBM}} = \sigma_K^M - 28\sigma_0 f(Z)/9. \tag{27}$$

The expansion (25) is supposed to be good for values of k less than 4. We have used it up to 7.404 MeV in order to obtain a smooth transition to values of σ_{DBM} calculated using the term contained in curly brackets in (12).

As can be seen from Table VI, the measured and measured mean values of σ_K for Bi differ from σ_K(calc) by less than the statistical errors. Indeed, up to 14 MeV the average discrepancy over 2 MeV intervals fluctuates between about +0.02% and −0.02%. Between 14 and 28 MeV it fluctuates between about +0.2% and −0.3%. Since the sum of the cross sections contained within the parentheses of (10) (which is about one-third as large as σ_K) is uncertain to about 0.2% (possible systematic error) this agreement may be fortuitous. Combining the experimental statistical errors of about 0.6% we estimate an uncertainty of 0.4% in the mean measured values. The various sources of uncertainty are summarized in Table VII. We conclude that σ_K(calc) and σ_K agree to within about (0.5 ± 0.4)% over the range of photon energies studied in this experiment. In the region of the giant dipole resonance the uncertainty in the discrepancy increases to about ±0.6% because of a possible 10% uncertainty in the nuclear absorption cross section. Some of the local deviations from σ_K(calc) may be significant, however. If we compare values of the pair cross section σ_K measured only in the present experiment with σ_K(calc), we see from Tables III and IV that between 6 and 13 MeV σ_K is systematically the larger in both Ta and Bi. The average discrepancy is about $+2\Sigma$, where Σ is the standard deviation in a single measurement, and so is significant. For Ta between 13 and 17 MeV the average discrepancy in the cross section changes sign and decreases in magnitude to about -0.6Σ. However, the Mainz measurements for Ta are larger than σ_K(calc) by about the same amount, so above 13 MeV an average $\bar{\sigma}_K$ of the Ottawa and Mainz cross sections agrees very well with the values of Hubbell *et al.*[6], as mentioned earlier. At 6.418 MeV Moreh and Wand[1] obtained (12 777 ± 12) mb for the total cross section of Ta and (15 487 ± 15) mb for Bi. Corresponding values interpolated from our data are (12 819 ± 22) mb and (15 662 ± 32) mb. For Ta, the value of σ_K deduced from the Negev measurements lies 33 mb above σ_K(calc) while ours lies 75 mb above, whereas for Bi the Negev value lies 125 mb below σ_K(calc) and ours lies 50 mb above. Hence the resonance absorption results corroborate our measurement of σ_K for Ta, the mean of the two measured values being 0.42% larger than σ_K(calc) at 6.418 MeV. For Bi at this energy the mean of Ottawa and Negev measured values is 0.24% less than σ_K(calc). Indeed, all of our measured σ_K between 4.3 and 5.8 MeV are smaller than σ_K(calc).

SUMMARY AND CONCLUSIONS

To summarize, the experimental evidence is that σ_K(calc) for Al, overestimated by nearly

TABLE VII. Summary of uncertainties in measured quantities caused by factors which do not cancel in the ratio of absorbed to transmitted intensity. The photon energy is denoted by ω, the total absorption cross section by σ, the atomic cross section by σ_Z, and the pair cross section by σ_K.

Measured quantity	Uncertainty	Cause	Remarks
ω	±0.5% at 6 MeV	timing	data were lumped into
	±1.9% at 26 MeV	resolution	500 keV bins, however
ω	±(0.5 ± 0.2) %	energy calibration	includes possible drift
σ	±0.2% at 6 MeV	counting	includes background
	±1.0% at 26 MeV	statistics	uncertainty
σ	±0.03% or less	photon flux normalization	dependence on absorber position
σ	±0.1% or less	photon flux variation	
σ	±0.2%	mass/unit area of absorber	
σ	−0.18% for Al	photon	correction applied
	−0.08% for Bi	in scattering	correction not applied
σ	−0.04% to −0.08% for Al	air displacement by absorber	correction applied
σ_Z	±0.2% near GDR	10% uncertainty in photonuclear cross section	additional to uncertainties in σ
σ_K	±0.1% or less	0.2% uncertainty in $(\sigma_{pe}+\sigma_c+\sigma_R+\sigma_t)$	additional to uncertainties in σ_Z

2% at 4 MeV, reaches agreement with the data by 13 MeV; that σ_K(calc) for Ta is on the average about 0.8% too small between 6 and 13 MeV, and is correct at higher energies; and that for Bi, σ_K(calc) is about 0.3% too large between 4 and 6 MeV, about 0.7% too small between 6 and 13 MeV, and is correct at higher energies. It should be noted that for Ta between 11 and 17 MeV a possible overestimate of 10% in the total nuclear absorption cross section σ_n causes an overestimate of about 0.2% in σ_Z (and so in σ_K) and for Bi an overestimate ranging from 0.1 to 0.3% (because of its narrower giant dipole resonance). If σ_n were in fact 10% smaller than believed, the conclusion that σ_K(calc) is too small would not be changed. Presumably the empirical Coulomb correction is the cause of these discrepancies, and since it contributes about 10% to the total cross section at intermediate energies it may be as much as 8% too small between 6 and 13 MeV for Ta and 7% for Bi.

Until calculations for σ_K are performed for heavy elements using exact Coulomb corrections between 5 and 50 MeV, values of σ_Z accurate to better than 1% will only be obtained by experiment. Nevertheless we conclude that the improved calculations[6] of the e^+-e^- pair cross sections give impressive agreement with experiment, albeit using an empirical Coulomb correction. The improved screening and Coulomb corrections used in these calculations are necessary to remove discrepancies as large as 3% in the older calculations of the pair cross section. In view of the close similarity of the matrix element for bremsstrahlung to that for pair production, we expect that bremsstrahlung cross sections of heavy elements will also require revision.

ACKNOWLEDGMENTS

We gratefully acknowledge a wide range of technical support provided by A. Nowak, M. Kosaki, and D. Kleinbub. We thank J.-P. Carlos for his collaboration during preliminary data taking. G. Hennek assisted in the engineering design of the LD_2 tank. B. Wheeler contributed to the mechanical design. Much of the mechanical construction was done in the NRC Physics Shop under the direction of W. Taylor, and some in the NRC Manufacturing and Technology Centre. The masses of the absorbers were measured by P. G. R. Gendron of the Mechanical and Optical Physics section.

APPENDIX A: COUNTING LOSS CORRECTIONS

The counting system shown schematically in Fig. 1 permits one neutron event to be recorded

after each Linac beam pulse. An early event stopping the time-to-digital converter (TDC) prevents observation of any later event produced by the same beam pulse. With the Linac operating at 720 Hz typically about 8000 events were recorded during each 1-min period when the full LD_2 target was irradiated without absorber (133 events/s). Total counting losses in this (worst) case were 3.4%, distributed over 1000 time channels. The greatest fractional counting loss (about 18%) occurred in the last channel, whereas the loss in the early channels was negligible. The TOF spectra were roughly bell shaped with a broad maximum in the counting rate per time channel occurring at a neutron energy of about 3 MeV. The region of interest corresponding to high energy neutrons lay mainly on the early side of the maximum. Counting losses in these channels were lower than at 3 MeV where the average losses were about 9% without absorber and 3% with absorber. If no dead-time correction were applied these losses would cause the absorption cross section at a photon energy of 8 MeV to appear to be about 5% too low (assuming 33% of the 8 MeV photons are transmitted by the absorber).

The observed count O_i in the ith time channel is

$$O_i = S\exp\left(-\sum_{j=1}^{i-1} C_j/S\right)(C_i/S)\exp(-C_i/S), \quad \text{(A1)}$$

where S is the total number of beam pulses used in the experiment. The first exponential term expresses the reduced probability of the TDC reaching the ith channel because of the cumulative probability than an event will occur in an earlier jth channel. Rewriting (A1) gives

$$C_i \exp(-C_i/S) = O_i \exp\left(\sum_{j=1}^{i-1}(C_j/S)\right). \quad \text{(A2)}$$

The present TOF data were corrected for dead-time channel by channel starting from the earliest, assuming that $\exp(-C_i/S)$ had the value unity, neglecting self-losses in the ith channel. This approximation causes a negligible systematic error which can be determined from the first-order approximation. Substituting $(1 - C_i/S)$ for $\exp(-C_i/S)$ and Y_i for the term on the right-hand side, (A2) becomes

$$C_i - C_i^2/S = Y_i. \quad \text{(A3)}$$

Where Y_i differs little from C_i, it can replace C_i in the quadratic term, so that

$$C_i = Y_i(1 + Y_i/S). \quad \text{(A4)}$$

At the maximum point in the TOF spectrum in the worst case, Y_i/S was about 8×10^{-4}. Including the self-loss correction increases the count per channel without absorber by 0.08% and the count with absorber by 0.03% which (because the absorber cross section is proportional to the logarithm of the ratio of the two counts) represents a 0.05% increase in the cross section at low energy.

The data presented here were accumulated in 13 separate runs. All the runs were added together and then corrected for counting losses. This procedure was justified by the observation that fluctuations from the average counting rate during a single run were similar to the fluctuation in average rate from run to run. For the full LD_2 target without absorber the weighted sum, (8236 ± 1221) events/min, of the average counting rates during the individual runs in the Al data set (each individual rate weighted by the ratio of the number of counting cycles in the run to the total number of cycles in the complete data set) differed from the mean of all the observations of the rate during all the runs, (8013 ± 899) events/min, by less than 3%. For this analysis the average counting rate during an individual run was determined from a series of separate readings taken at random times.

To estimate the possible systematic error introduced by a global dead-time correction, we have compared the cross section for Al at low energy computed from an additional run of 885 cycles duration (about 88.5 beam hours) with the cross section obtained from the sum of the present set of runs with Al absorber, amounting to 3047 cycles, as shown in Table V.

An increase by 20% in the observed counting rate from the average rate requires dead-time corrections of 11% at the maximum of the TOF spectrum of LD_2 without absorber and 4% at the maximum of the spectrum with absorber, compared to 7% and $2\frac{1}{2}$% for a counting rate 20% below average. The same given ratio of "absorber-in" to "absorber-out" counts in the maximum channel, corrected for dead time according to these two different rates, would give values of the cross section differing by about ±1.5%. This figure is an upper limit to the possible error since a dead-time correction based on the average counting rate will be quite appropriate for about half of the data.

In the 885-cycle run the average neutron counting rate was (8460 ± 858) events/min where the quoted error is the average of the absolute values of the deviations from the mean of 51 readings recorded at different times during the run. This is 4% higher than the average rate of (8172 ± 947) events/min for the remaining Al runs. The absorption cross sections for Al extracted from the two different data sets are compared in Table V at low energies. We see for example that at 7.936 MeV the two values (1.085 ± 0.004) b and (1.089

±0.002) b differ by no more than 0.4%, which is less than the statistical uncertainty. One might therefore estimate that at energies as low as 8 MeV the possible error resulting from applying the dead-time correction globally to all the data could be about ±0.2%. However, the average difference between the two sets of measured cross sections over the photon energy interval 3.87 to 12.6 MeV is only +0.0013 b, which is a discrepancy of only 0.1%.

APPENDIX B: SCATTERING CORRECTIONS

At low energy the Compton scattering cross section σ_C is a large fraction of the total photon cross section σ. As the incident photon energy increases the fractional contribution of σ_C decreases. For Al, σ_C contributes 94.5% of σ at 3 MeV, and 52.5% at 15 MeV; while for Bi, σ_C is 64.3% of σ at 3 MeV, and 15.8% at 15 MeV. Some Compton-scattered photons, reduced in energy, remain within the detection solid angle causing an apparent reduction in the measured cross section at a lower energy. We can show, however, that the effect is quite small for Al, and negligible for Bi.

Because the solid angle subtended by the LD_2 target at the absorber was small, the energy ω' of photons scattered by the absorber through an angle θ_s into the target differed by only a small amount $\Delta\omega$ from the energy ω of the incident photon:

$$\Delta\omega = \omega[1 + k^{-1}(1 - \cos\theta_s)^{-1}]^{-1}, \tag{B1}$$

where $\Delta\omega = (\omega - \omega')$, $k = \omega/m$, and m is the mass energy of the electron. The bremsstrahlung entering the absorber was collimated into a cone whose apex half angle (0.55°) was slightly less than the angle subtended at the radiator by the exit end of the LD_2 target. The radiator was 1.34 m from the front face of the absorber and 2.49 m from the front face of the LD_2 target. For the Ta and Bi absorbers, each about 2.5 cm long, the maximum possible in-scattering angle θ_s^{max} was 2.5°. For the Al absorber (about 18 cm long) θ_s^{max} was 2.9°. Between the mid plane of the Al absorber and the center of the LD_2 target, θ_s could be no larger than 2.5°. The average solid angle for in-scattering was about 1.84 msr for the Al absorber.

Scattering by 2.5° reduces the energy of 10 MeV photons by 183 keV, of 20 MeV photons by 718 keV, and of 30 MeV photons by 1588 keV. The cross section for attenuation of a photon varies slowly with ω and is essentially the same before and after a small-angle scattering. The path length in the absorber traversed by a detected photon is very nearly the same whether or not scattering has occurred.

The differential cross section for scattering of unpolarized photons by electrons according to Klein and Nishina is

$$\frac{d\sigma_C(\omega)}{d\Omega} = (r_0^2/2)(\omega'/\omega)^2(\omega/\omega' + \omega'/\omega - \sin^2\theta_s), \tag{B2}$$

where r_0 is the classical radius of the electron. For $\theta_s \sim 2°$, so that $\sin\theta_s \sim 10^{-3}$, (B2) can be written as

$$\frac{d\sigma_C(\omega)}{d\Omega} \simeq r_0^2(\omega'/\omega)(1 - \Delta\omega/\omega) \tag{B3}$$

and hence as

$$\frac{d\sigma_C(\omega)}{d\Omega} \simeq r_0^2(1 - \Delta\omega/\omega)(1 - 2\Delta\omega/\omega). \tag{B4}$$

At 10 MeV, $d\sigma_C/d\Omega$ can fall to about 0.94 r_0^2, and at 30 MeV it can fall to about 0.84 r_0^2, when σ_C is as large as 2.5°. It is a slight overestimate therefore, for an absorber of atomic number Z, to use Z times the zero-angle differential scattering cross section for hydrogen ($r_0^2 = 79.41$ mb) as the forward-scattering differential cross section averaged over the detection solid angle:

$$\left(\frac{d\sigma_C}{d\Omega}\right)_Z = 79.41Z \ (\text{mb sr}^{-1}).$$

The effect of in-scattering thought of as a (negative) cross section "σ_s" can therefore be expressed as a fraction of $\sigma(\omega)$ by

$$(\text{"}\sigma_s\text{"}/\sigma(\omega))_Z \simeq \left(\frac{d\sigma_C}{d\Omega}\right)_Z \Delta\Omega/\sigma(\omega). \tag{B5}$$

For Al at 10 MeV, where σ is 1.037 b, the effect is smaller than 0.18%. In the case of Bi at 10 MeV, in-scattering can reduce the cross section observed in this experiment by no more than 0.08%, and by lesser amounts at higher energies. Even at 10 MeV this correction is three times smaller than the statistical error in the experimental value, and is an even smaller fraction of it at lower or higher energies. Hence no correction has been applied to the Ta and Bi cross sections.

*Present address: Australian Radiation Laboratory, Melbourne, Australia.

[1]R. Moreh, D. Salzmann, and Y. Wand, Phys. Lett. 30B, 536 (1969); T. Bar-Noy, Internal Report, Nuclear Research Center, Negev, Beer-Sheba, Israel; R. Moreh and Y. Wand, Nucl. Phys. A252, 423 (1975).

[2]S. Sugiyama and T. Tomimasu, *Proceedings of the International Conference on Photonuclear Reactions and Applications*, edited by B. L. Berman (University of California, Livermore, 1973), Vol. I, p. 563.

[3]J. Ahrens, H. Borchert, K. H. Czock, H. B. Eppler, H. Gimm, H. Gundrum, M. Kroning, P. Riehn, G. Sita Ram, A. Zieger, and B. Ziegler, Nucl. Phys. A251, 479 (1975).

[4]J. H. Hubbell, Report No. NSRDS-NBS 29 (U. S. Government Printing Office, Washington, 1969), p. 1.

[5]E. Storm and H. I. Israel, Nucl. Data Tables A7, 565 (1970).

[6]H. A. Gimm and J. H. Hubbell, National Bureau of Standards Technical Note 968 (U.S. Government Printing Office, Washington, 1978), p. 4; and J. H. Hubbell, H. A. Gimm, and I. Øverbø (private communication).

[7]I. Øverbø, Phys. Lett. 71B, 412 (1977).

[8]For a review, see N. K. Sherman, Nucl. Instrum. Methods 116, 301 (1974).

[9]C.-P. Wu, F. W. K. Firk, and B. L. Berman, Nucl. Instrum. Methods 79, 346 (1970).

[10]R. G. Jones, R. G. Johnson, J. W. Jury, J. I. Lodge, K. H. Lokan, N. K. Sherman, and R. W. Gellie, Phys. Can. 27, 59 (1971); and R. G. Jones, M.Sc thesis Trent University, 1971 (unpublished).

[11]J. Ahrens, H. Borchert, A. Zieger, and B. Ziegler, Nucl. Instrum. Methods 108, 517 (1973).

[12]N. K. Sherman, Nucl. Instrum. Methods 79, 197 (1970).

[13]L. C. Henry and T. J. Kennett, Can. J. Phys. 49, 1167 (1971).

[14]R. R. Harvey, J. T. Caldwell, R. L. Bramblett, and S. C. Fultz, Phys. Rev. 136, B126 (1964).

[15]L. M. Young, Ph.D. thesis University of Illinois, 1972 (unpublished).

[16]R. L. Bramblett, J. T. Caldwell, G. F. Archampaugh, and S. C. Fultz, Phys. Rev. 129, 2723 (1963).

[17]R. Bergère, H. Beil, and A. Veyssière, Nucl. Phys. A121, 463 (1968).

[18]For a review, see J. W. Motz, H. A. Olsen, and H. W. Koch, Rev. Mod. Phys. 41, 581 (1969).

[19]L. C. Maximon, J. Res. Natl. Bur. Stand. 72B, 79 (1968).

[20]L. C. Maximon and H. A. Gimm, National Bureau of Standards Internal Report 78-1456 (U.S. Government Printing Office, Washington, 1978), p. 9.